All-Electric Access to the Magnetic-Field-Invariant Magnetization of Antiferromagnets

Tobias Kosub,[1] Martin Kopte,[1] Florin Radu,[2] Oliver G. Schmidt,[1] and Denys Makarov[1,*]

[1]*Institute for Integrative Nanosciences, IFW Dresden, 01069 Dresden, Germany*
[2]*Helmholtz-Zentrum Berlin, 14109 Berlin, Germany*

The rich physics of thin film antiferromagnets can be harnessed for prospective spintronic devices given that all-electric assessment of the tiny uncompensated magnetic moment is achieved. On the example of magnetoelectric antiferromagnetic Cr_2O_3, we prove that spinning-current anomalous Hall magnetometry serves as an all-electric method to probe the field-invariant uncompensated magnetization of antiferromagnets. We obtain direct access to the surface magnetization of magnetoelectric antiferromagnets providing a read-out method for ferromagnet-free magnetoelectric memory. Owing to the great sensitivity, the technique bears a strong potential to address the physics of antiferromagnets. Exemplarily, we apply the method to access the criticality of the magnetic transition for an antiferromagnetic thin film. We reveal the presence of field-invariant uncompensated magnetization even in 6-nm-thin IrMn films and clearly distinguish two contributions, of which only the minor one is involved in interfacial magnetic coupling. This approach is likely to advance the fundamental understanding of the anomalous Hall and magnetic proximity effects.

Antiferromagnetic exchange coupling in materials unites magnetic order with vanishing magnetization and low magnetic susceptibility. This peculiar combination has recently triggered a reexamination of antiferromagnets [1,2] in the scope of prospective spintronic devices that are robust against magnetic disturbances [3,4] and operate up to terahertz frequencies [5]. The tiny uncompensated magnetic moment of the locally uncompensated antiferromagnetic lattice determines the topology of antiferromagnetic domain walls [6], the control of which [7] could peak in antiferromagnetic analogues to racetrack devices [8]. Furthermore, the uncompensated antiferromagnetic moment is the key element of artificial multiferroics based on heterostructures of magnetoelectric antiferromagnets and ferromagnets, which form the core of novel magnetoelectric random access memory (MERAM) devices [9]. While the all-electric read-out of the magnetic field response of the linear antiferromagnetic order parameter has been demonstrated using the anisotropic and spin Hall magnetoresistance effects [10], the all-electric read-out of the uncompensated moment of antiferromagnets is a notoriously difficult task. In contrast to ferro-and ferrimagnets, the magnetic moment is very small and usually invariant with respect to applicable magnetic fields [11].

One of the most sensitive techniques for thin film magnetometry utilizes the anomalous Hall effect (AHE) [12] to monitor the magnetization-proportional anomalous Hall resistance in varying magnetic fields. The Hall response typically suffers from a sizable parasitic signal offset due to imperfect device geometry. If the measured hysteresis loops contain no field-invariant moment—i.e., *full loops* [right side of Fig. 1(a)]—it is justified to remove this residual signal offset by manually centering the loop at

zero signal. When the necessary magnetic fields for full loops are not reached—i.e., *minor loops* are measured [left side of Fig. 1(a)]—the manual centering of the loop destroys the important information about the field-invariant moment. Thus, conventional AHE magnetometry can only quantify invariant magnetization after entirely erasing it. For antiferromagnets, such erasing fields can be several Tesla, which makes their invariant magnetization effectively invisible to conventional AHE magnetometry.

Spinning-current anomalous Hall magnetometry.— Here, we extend the capabilities of AHE magnetometry to beyond these limitations and carry out precise measurements of field-invariant antiferromagnetic magnetization. By applying the spinning-current approach [13], the parasitic signal contributions to the Hall signal are dynamically compensated and the pure quantitative Hall signal is always recovered including any field-invariant components. The underlying principle is that the parasitic offset changes sign if the four Hall contacts are cyclically permuted. Thus, continuous cyclical permutation of the terminals yields zero average parasitic signal offset (Supplemental Material [14], Sec. I). The measurement scheme is realized by the combination of a 4×4 matrix multiplexer and a four-terminal AHE magnetometry setup which makes the proposed technique immediately available to many laboratories throughout the world.

As this method is based on the anomalous Hall effect, the measures are products of the sample magnetization and the anomalous Hall coefficient. When systems belonging to the *good-metal regime* [12,17] are investigated, the anomalous Hall coefficient can be assumed to be independent of the sample resistance. In this regime, the measured Hall resistances can be treated as semiquantitative magnetization
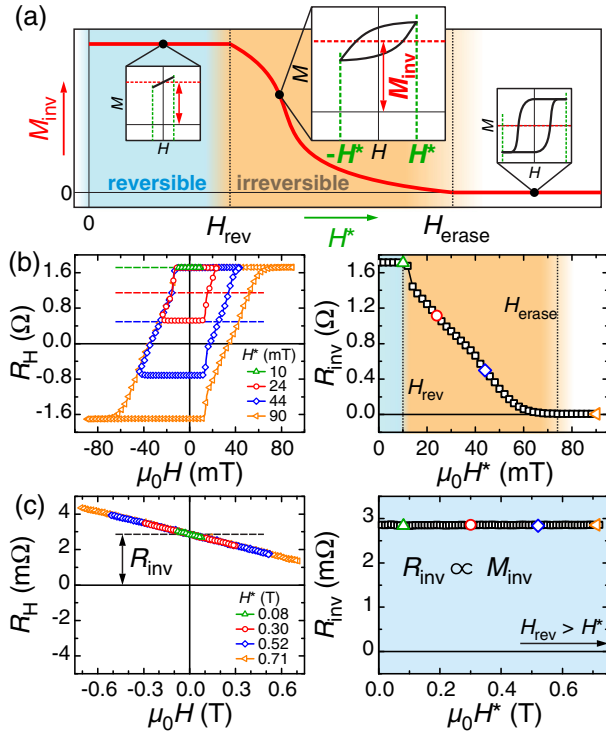
FIG. 1 (color online). (a) Sketch of the dependence of field-invariant magnetization M_{inv} on the actually employed maximum field H^*. The insets show representative hysteresis loops. (b) Evolution of the minor hysteresis loops and invariant magnetization with H^* for a ferromagnetic Co(0.8 nm)/Pt thin film. (c) The same as (b), but for an antiferromagnetic Cr_2O_3(250 nm)/Pt layer with field-invariant magnetization up to the highest H^* achievable.

values which apply for the samples discussed in the present study. Systems outside the good-metal regime can be investigated, while care has to be taken that changes of the anomalous Hall coefficient can distort the observed dependences.

When applied to ferromagnetic thin films [Fig. 1(b)], this technique allows one to unambiguously locate minor within full loops. The according field-invariant moment (i.e., vertical offset) of the loop as a function of the maximum field can be readily extracted resembling the scheme shown in Fig. 1(a). While similar measurements are possible with conventional AHE magnetometry by manual centering of the full loop, the potential of the spinning-current method becomes evident when attempting to carry out such measurements for an antiferromagnetic sample [Fig 1(c)]: Although we cannot reach the erasing field, it is possible to measure the dependence of the field-invariant signal.

We demonstrate the technique by carrying out measurements for two distinct antiferromagnets: (a) 250-nm-thick single-orientation films of highly crystalline insulating Cr_2O_3 with uniaxial anisotropy which is a magnetoelectric antiferromagnet and (b) 6-nm-thick metallic polycrystalline films of IrMn which play a crucial role in magnetic spin

valves. For IrMn samples, we additionally investigate an exchange bias system [11,18] using a [Pt(0.8 nm)/Co(0.5 nm)]$_4$ multilayer stack with an out-of-plane magnetic easy axis as the ferromagnetic layer. All samples were patterned lithographically to obtain cross-structured samples with 30–1000 μm line width. Further details on sample preparation and electric measurements are given in Supplemental Material [14], Sec. II.

The measurement protocol regarding the field-invariant antiferromagnetic magnetization is as follows: The sample is first warmed to T_{max}. Then, with the magnetic cooling field H_{cool} applied perpendicular to the sample surface, the sample is cooled to a temperature below the desired measurement temperature, which is finally approached from the cold side. The actual determination of $R_{inv}(T, H_{cool})$ is then carried out in zero magnetic field. Therefore, contributions from the normal Hall effect, spin Hall, and anisotropic magnetoresistance are excluded. The initial warming temperature $T_{max} = 45\,°C$ is chosen well above the bulk Néel temperature of the Cr_2O_3 of $T_N \approx 37\,°C$ [19], below which one of two possible magnetic order parameters along the c axis is selected [20]. For films with polycrystalline IrMn antiferromagnets, the warming ensured a partial unblocking of some IrMn grains, which are then susceptible to the field-cooling treatment [21].

Antiferromagnetic Cr_2O_3.—First, we address measurements of the surface magnetization of antiferromagnetic Cr_2O_3, which is a stable feature of the lattice termination for magnetoelectric antiferromagnets [22,23]. Cr_2O_3 is also an electric insulator and is a prototype material for the realization of MERAM devices [9,19,24]. To assess its magnetic properties via AHE magnetometry, we make use of the magnetic proximity effect in Pt [25] to create a magnetization within the 2-nm-thick conductive Pt layer that is probed by the AHE [Fig. 2(a)]. A control study on Cr_2O_3/Au is provided in Supplemental Material [14], Sec. III. Figure 2(b) shows hysteresis loops measured at several temperatures above and below the thin film Néel temperature of $T_N \approx 28\,°C$ [24] after magnetic field cooling in $\mu_0 H_{cool} = 0.6\,T$. The contributions from invariant magnetization shift the hysteresis loop away from the zero level along the *vertical* (Hall resistance) axis. This invariant signal appears only below the Néel temperature [Fig. 2(c)], hinting clearly at its origin in the uncompensated magnetic moment at the surface of the Cr_2O_3 film. From the magnetic transition region, we can extract a critical exponent of $\beta = 0.327 \pm 0.013$, which is close to the criticality for bulk Cr_2O_3 at $\beta = 0.314$ [26] (Supplemental Material [14], Sec. IV). To this end, spinning-current AHE magnetometry provides a way to study the criticality of the magnetic transition for antiferromagnetic thin films that are too thin to employ neutron diffraction.

Furthermore, we access the invariant surface magnetization of Cr_2O_3 in dependence of the cooling field [Fig. 2(d)]. The nonzero signal unambiguously indicates
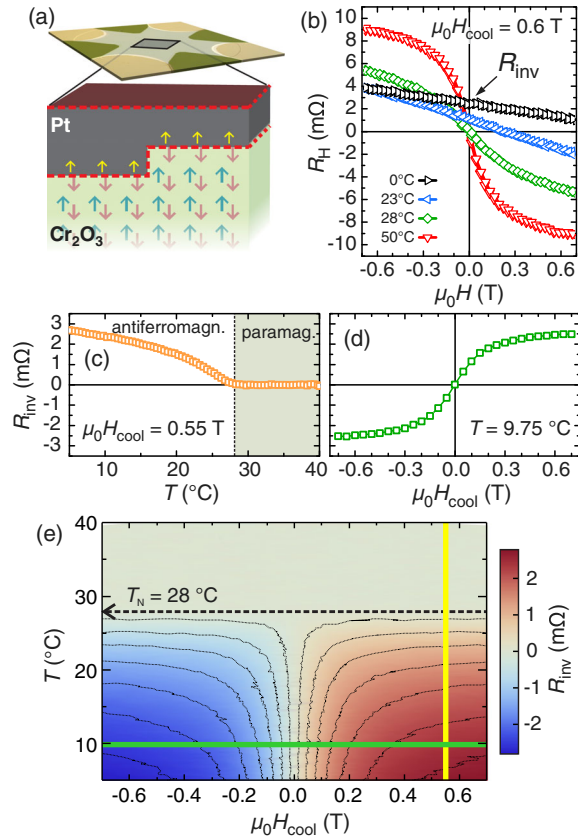
FIG. 2 (color online).   (a) The AHE measurements on insulating Cr_2O_3 exploit its uncompensated surface and the magnetic proximity effect in platinum. (b) Hysteresis loops obtained by spinning-current anomalous Hall magnetometry at various temperatures above and below the thin film Néel temperature of $T_N \approx 28$ °C. (c),(d) Temperature and cooling field dependence of the invariant magnetization at the Cr_2O_3 surface, respectively. (e) Full map of the invariant magnetization over the T-H_{cool} space. The crosscuts of (c) and (d) are indicated as colored lines.

a surplus of either positive or negative surface magnetization, which is correlated with an abundance of one bulk order parameter over the antiparallel one in this material class [20,22,23]. This purely magnetic-field-driven antiferromagnetic domain selection is theoretically not allowed in perfect Cr_2O_3, which hints to a parasitic effect in thin films that could interfere with the magnetoelectric bit writing process in MERAMs [9]. The all-electric acquisition allows time-efficient and precise multiparametric maps of the invariant magnetization signal. The 2D map of $R_{inv}(T, H_{cool})$ around the critical ($T = T_N$, $H_{cool} = 0$) point shown in Fig. 2(e) was acquired in a few hours only with a high level of detail [Figs. 2(c) and 2(d) are taken from the map]. These performance parameters are superior to those of conventional techniques like superconducting quantum interference devices, cryogenic magnetic force microscopy, and synchrotron-based x-ray magnetic dichroism experiments.

Remarkably, the performed measurements demonstrate the all-electric read-out of the antiferromagnetic domain state of magnetoelectric Cr_2O_3 without using a ferromagnetic layer [19,24]. This is substantial progress to bring MERAMs closer to application [27] as the ferromagnetic layer used as the magnetic indicator imposes substantial writability problems [28] and fails to reliably indicate the antiferromagnetic domain state [19,24].

IrMn exchange bias system.—In the following, we apply the spinning-current anomalous Hall magnetometry to investigate polycrystalline IrMn antiferromagnets. Such films are widely employed technologically in exchange bias applications such as magnetic memory devices [21]. Figure 3(a) shows a typical exchange bias *minor* loop measured for the $[Pt/Co]_4$/IrMn exchange bias system that is characterized by loop shifts along the magnetic field direction H_{shift} and the vertical direction R_{inv}. The latter is visible by overlaying the two saturation branches [lower panel in Fig. 3(a)]. The vertical shift results from the invariant magnetization of the antiferromagnet, and the horizontal loop shift H_{shift} is a trait of the ferromagnetic film. It is widely accepted that the horizontal loop shift is influenced by the field-invariant moment of the pinning antiferromagnet [11,18,21] responsible for the vertical loop shift. This field-invariant uncompensated moment is induced by cooling under exchange coupling to the ferromagnet [29].
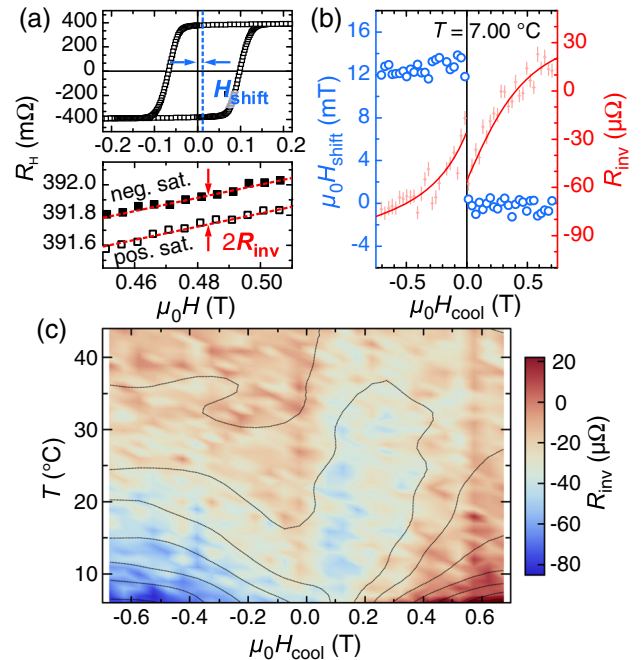
FIG. 3 (color online).   (a) Extraction method of the horizontal shift H_{shift} and the vertical shift R_{inv} from an experimental hysteresis loop of the $[Pt/Co]_4$/IrMn exchange-biased samples measured using spinning-current AHE magnetometry. (b) Dependence of both parameters on the cooling field H_{cool}. Lines are guides for the eye. (c) Full map of the invariant magnetization signal over the T-H_{cool} space.

Spinning-current AHE magnetometry is able to provide measurements of both the horizontal and the vertical loop shifts, which is beyond the precision obtained in a vibrating sample magnetometer (Supplemental Material [14], Sec. V). Figure 3(b) summarizes both horizontal and vertical loop shifts of the $[Pt/Co]_4/IrMn$ exchange bias system in dependence of the magnetic cooling field. The ferromagnetic $[Pt/Co]_4$ layer was always saturated along the cooling field direction during the field-cooling process. Note that a part of the antiferromagnet was set during the sample preparation and remains blocked even at the hot end of the measurement window ($T_{max} = 45\,°C$). This introduces a general bias towards positive horizontal and negative vertical loop shifts. The horizontal hysteresis loop shift H_{shift} appears to be independent of the cooling field within the field ranges probed here. Instead, it is dominated by the exchange with the ferromagnetic layer which dictates the exchange bias direction during the cooldown [29] resulting in the pronounced jump when the cooling field and the ferromagnet are reversed. The vertical loop shift represents the integral field-invariant magnetization of the IrMn layer which reveals two contributions: (i) The jump at zero is caused by the imprint of magnetization by the ferromagnet [29]. (ii) There is additional field-invariant magnetization in the antiferromagnet that is induced by the magnetic cooling field and not by exchange coupling. Consequently, this latter magnetization is not correlated with the magnitude of the exchange dominated horizontal loop shift.

The distinguished identification of the two contributions to the invariant magnetization suggests a depth dependence of the invariant magnetization close to the interface [30]. Based on the single sample investigated here, we conclude that the influence depth of the interfacial exchange is significantly lower than the total thickness of the IrMn of 6 nm. By thickness-dependent tests, this figure could be further constrained. Such investigations can fundamentally contribute to the understanding of polycrystalline antiferromagnets and the nanoscopic processes at play in exchange bias coupling.

Figure 3(c) provides an extended map of the invariant magnetization signal in the $[Pt/Co]_4/IrMn$ system. While it is qualitatively similar to the map acquired for Cr_2O_3, there is a noteworthy distinction: The invariant signal does not vanish for high temperatures. This is caused by the wide blocking temperature distribution of the polycrystalline thin film of IrMn [21]. Further analysis of the blocking temperature distribution is provided in Supplemental Material [14], Sec. VI. The magnitude of the observed invariant signal is substantially lower in the IrMn samples compared to that obtained for Cr_2O_3/Pt, because the field-invariant magnetization is not strictly aligned out of plane and the conductive part of the sample is much thicker shunting the Hall signal.

Plain antiferromagnetic IrMn.—The high sensitivity and stability of all-electric measurements allow one even to
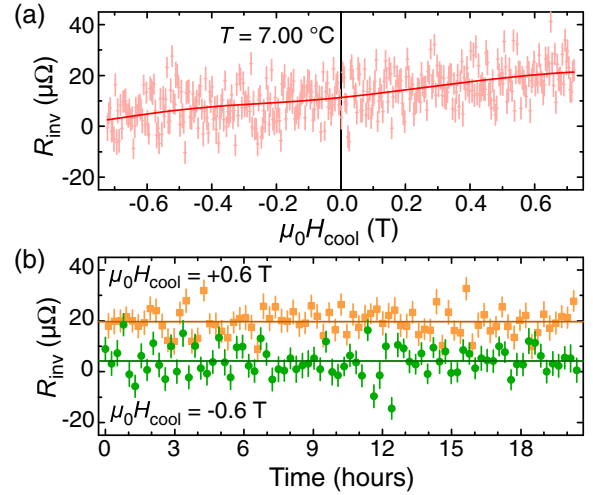
FIG. 4 (color online). (a) Cooling field dependence of the invariant magnetization signal of the plain IrMn system at $T = 7\,°C$. The line is a filtered version of the data. (b) Consecutive measurements at $\mu_0 H_{cool} = +0.6$ T and -0.6 T, alternatingly, showing a signal difference at 20σ significance.

measure cooling field dependences of the tiny uncompensated magnetization in a plain 6-nm-thick IrMn sample with no exchange bias coupling. To the best of our knowledge, no such measurements have been performed before. In contrast to the cooling field dependence of the field-invariant magnetization for the $[Pt/Co]_4/IrMn$ system [Fig. 3(b)], the lack of a ferromagnet in the plain IrMn sample generates a monotonic cooling field dependence [Fig. 4(a)]. To further corroborate these measurements, Fig. 4(b) shows consecutive and alternating measurements done after field cooling in $\mu_0 H_{cool} = \pm 0.6$ T measured continuously. The detected signal difference is unambiguous with a significance of 20σ (Supplemental Material [14], Sec. VII). This proves that invariant magnetization is induced in polycrystalline thin film antiferromagnets even in the absence of exchange bias by magnetic field cooling. This result also explains the cooling-field-dependent variation of the invariant signal observed for the exchange-biased $[Pt/Co]_4/IrMn$ system [Fig. 3(b)]. Possible reasons for the even smaller signal of the plain IrMn when compared to the $[Pt/Co]_4/IrMn$ system are growth-induced higher anisotropy and/or a lower anomalous Hall coefficient in the plain IrMn system.

Conclusion.—We proposed to use a spinning-current measurement layout in anomalous Hall effect magnetometry and showed that this opens the scope for magnetic phenomena that can go amiss in conventional Hall measurements with a stationary current direction. The adoption of this technique will therefore substantially improve the reach of lab-based transport investigations in the thriving field of antiferromagnetic spintronics, but also magnetoelectrics and topological effects.

We investigated both plain antiferromagnetic and ferromagnetic-antiferromagnetic systems using two rather

different antiferromagnets, namely, single-crystalline insulating Cr_2O_3 and polycrystalline metallic IrMn. For Cr_2O_3, we gained direct and all-electric access to the minute uncompensated surface magnetization, which makes feasible the novel concept of ferromagnet-free MERAMs [27]. The unprecedented precision allows one to identify parasitic effects interfering with the antiferromagnetic domain selection in this magnetoelectric material.

In metallic antiferromagnetic systems like IrMn, this lab-based technique represents a unique all-electric way to quantify the field-invariant magnetization responsible for the exchange bias effect. We reveal that not all of the invariant magnetization acts in the interfacial exchange coupling, which provides potential access to the exchange parameters of the exchange bias interface.

As the spinning-current method imposes fewer restrictions about measurement parameters and requires fewer assumptions about samples in AHE measurements, it is likely that the understanding of the AHE itself can be further improved [12] by measurements exploiting the dynamic spinning-current offset cancellation. The Cr_2O_3/metal system, in particular, provides a fascinating testbed for in-depth studies of the magnetic proximity effect (Supplemental Material [14], Sec. III). As the spins in the antiferromagnet are extremely stable in external magnetic fields [Fig. 1(d)], this technique allows for the magnetic proximity effect to be studied also in ferro- and ferrimagnets.

---

*d.makarov@ifw-dresden.de

[1] H. Chen, Q. Niu, and A. H. MacDonald, Phys. Rev. Lett. **112**, 017205 (2014).

[2] W. Zhang, M. B. Jungfleisch, W. Jiang, J. E. Pearson, A. Hoffmann, F. Freimuth, and Y. Mokrousov, Phys. Rev. Lett. **113**, 196602 (2014).

[3] J. Železný, H. Gao, K. Výborný, J. Zemen, J. Mašek, A. Manchon, J. Wunderlich, J. Sinova, and T. Jungwirth, Phys. Rev. Lett. **113**, 157201 (2014).

[4] R. Cheng, J. Xiao, Q. Niu, and A. Brataas, Phys. Rev. Lett. **113**, 057601 (2014).

[5] T. Kampfrath, A. Sell, G. Klatt, A. Pashkin, S. Mährlein, T. Dekorsy, M. Wolf, M. Fiebig, A. Leitenstorfer, and R. Huber, Nat. Photonics **5**, 31 (2011).

[6] M. Bode, E. Vedmedenko, K. Von Bergmann, A. Kubetzka, P. Ferriani, S. Heinze, and R. Wiesendanger, Nat. Mater. **5**, 477 (2006).

[7] E. G. Tveten, A. Qaiumzadeh, and A. Brataas, Phys. Rev. Lett. **112**, 147204 (2014).

[8] S. S. Parkin, M. Hayashi, and L. Thomas, Science **320**, 190 (2008).

[9] A. Hochstrat, X. Chen, P. Borisov, and W. Kleemann, U.S. Patent 7719883 B2 (2005).

[10] X. Marti et al., Nat. Mater. **13**, 367 (2014).

[11] F. Radu and H. Zabel, Springer Tracts Mod. Phys. **227**, 97 (2008).

[12] N. Nagaosa, J. Sinova, S. Onoda, A. MacDonald, and N. Ong, Rev. Mod. Phys. **82**, 1539 (2010).

[13] P. Daniil and E. Cohen, J. Appl. Phys. **53**, 8257 (1982).

[14] See Supplemental Material at http://link.aps.org/supplemental/10.1103/PhysRevLett.115.097201 for sample fabrication, spinning-current offset cancellation method, data evaluation for Cr_2O_3 and IrMn samples, which includes Refs. [15,16].

[15] D. Qu, S. Huang, J. Hu, R. Wu, and C. Chien, Phys. Rev. Lett. **110**, 067206 (2013).

[16] T. Kosub, A. Bachmatiuk, D. Makarov, S. Baunack, V. Neu, A. Wolter, M. H. Rümmeli, and O. G. Schmidt, J. Appl. Phys. **112**, 123917 (2012).

[17] T. Miyasato, N. Abe, T. Fujii, A. Asamitsu, S. Onoda, Y. Onose, N. Nagaosa, and Y. Tokura, Phys. Rev. Lett. **99**, 086602 (2007).

[18] J. Nogués and I. K. Schuller, J. Magn. Magn. Mater. **192**, 203 (1999).

[19] X. He, Y. Wang, N. Wu, A. N. Caruso, E. Vescovo, K. D. Belashchenko, P. A. Dowben, and C. Binek, Nat. Mater. **9**, 579 (2010).

[20] P. Brown, J. Forsyth, and F. Tasset, J. Phys. Condens. Matter **10**, 663 (1998).

[21] K. O'Grady, L. Fernandez-Outon, and G. Vallejo-Fernandez, J. Magn. Magn. Mater. **322**, 883 (2010).

[22] K. D. Belashchenko, Phys. Rev. Lett. **105**, 147204 (2010).

[23] N. Wu, X. He, A. L. Wysocki, U. Lanke, T. Komesu, K. D. Belashchenko, C. Binek, and P. A. Dowben, Phys. Rev. Lett. **106**, 087202 (2011).

[24] T. Ashida, M. Oida, N. Shimomura, T. Nozaki, T. Shibata, and M. Sahashi, Appl. Phys. Lett. **104**, 152409 (2014).

[25] Y. Lu, Y. Choi, C. Ortega, X. Cheng, J. Cai, S. Huang, L. Sun, and C. Chien, Phys. Rev. Lett. **110**, 147207 (2013).

[26] U. Köbler and A. Hoser, Renormalization Group Theory (Springer, New York, 2009).

[27] T. Kosub, O. G. Schmidt, and D. Makarov, patent pending.

[28] K. Toyoki, Y. Shiratsuchi, A. Kobane, S. Harimoto, S. Onoue, H. Nomura, and R. Nakatani, J. Appl. Phys. **117**, 17D902 (2015).

[29] G. Salazar-Alvarez, J. J. Kavich, J. Sort, A. Mugarza, S. Stepanow, A. Potenza, H. Marchetto, S. S. Dhesi, V. Baltz, B. Dieny, A. Weber, L. J. Heyderman, J. Nogués, and P. Gambardella, Appl. Phys. Lett. **95**, 012510 (2009).

[30] S. Mishra, F. Radu, S. Valencia, D. Schmitz, E. Schierle, H. Dürr, and W. Eberhardt, Phys. Rev. B **81**, 212404 (2010).